

Oxidative Reactivity of (N2S2)PdRX Complexes (R = Me, Cl; X = Me, Cl, Br): Involvement of Palladium(III) and Palladium(IV) Intermediates

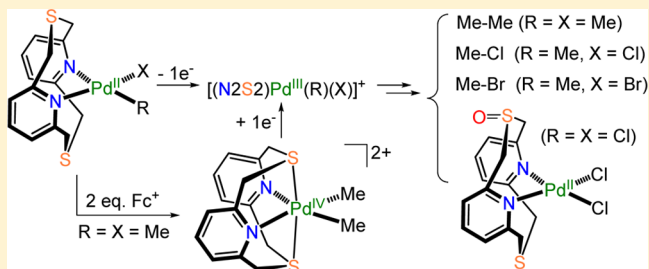
Jia Luo,[†] Nigam P. Rath,[‡] and Liviu M. Mirica^{*,†}

[†]Department of Chemistry, Washington University, One Brookings Drive, St. Louis, Missouri 63130-4899, United States

[‡]Department of Chemistry and Biochemistry, One University Boulevard, University of Missouri–St. Louis, St. Louis, Missouri 63121-4400, United States

Supporting Information

ABSTRACT: A series of (N2S2)PdRX complexes (N2S2 = 2,11-dithia[3.3](2,6)pyridinophane; R = X = Me, **1**; R = Me, X = Cl, **2**; R = Me, X = Br, **3**; R = X = Cl, **4**) were synthesized, and their structural and electronic properties were investigated. X-ray crystal structures show that for the corresponding Pd(II) complexes the N2S2 ligand adopts a κ^2 conformation, with the pyridine N donors binding in the equatorial plane. Cyclic voltammetry (CV) studies suggest that the Pd(III) oxidation state is accessible at moderate redox potentials. In situ EPR, ESI-MS, UV–vis, and low-temperature electrochemical studies were employed to detect the formation of Pd(III) species during the oxidation of Pd(II) precursors. In addition, the [(N2S2)Pd^{IV}Me₂](PF₆)₂ ([1²⁺](PF₆)₂) complex was isolated by oxidation of **1** with 2 equiv of FcPF₆, and its structural characterization reveals an octahedral Pd(IV) center. The reversible Pd^{IV/III} redox couple for the Pd(IV) species supports the observed formation of the Pd(III)–dimethyl species upon chemical reduction of 1²⁺. In addition, reactivity studies reveal ethane, MeCl, and MeBr elimination upon one-electron oxidation of **1** (as well as the one-electron reduction of 1²⁺), **2**, and **3**, respectively. Mechanistic studies suggest the initial formation of a Pd(III) species, followed by methyl group transfer/disproportionation and subsequent reductive elimination from a Pd(IV) intermediate, although a halogen radical pathway cannot be completely excluded during C–halide bond formation. Interestingly, computational results suggest that the N2S2 ligand stabilizes to a greater extent the Pd(IV) vs the Pd(III) oxidation state, likely due to steric rather than electronic effects.

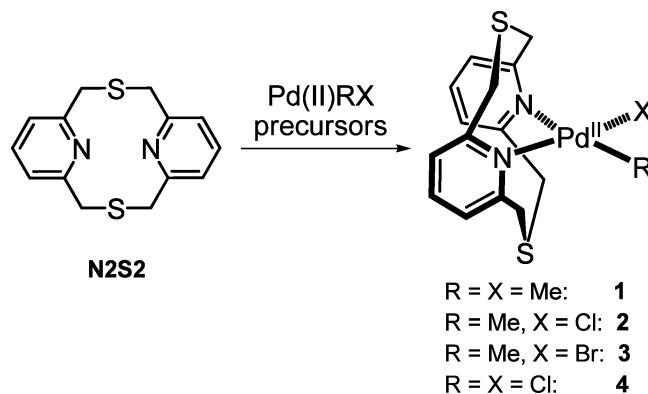


INTRODUCTION

Pd-catalyzed transformations are being extensively utilized in C–C and C–heteroatom bond formation reactions,^{1–3} as key steps in target-oriented syntheses to afford complex natural products, functional advanced materials, pharmaceuticals, and other high-value chemicals.⁴ While the common Pd oxidation states involved in these catalytic cycles are Pd(0) and Pd(II),^{5–8} Pd(III) and Pd(IV) species are also proposed as reactive intermediates,^{2–4,9–12} yet they have been less commonly isolated and characterized.^{13–21} We have recently reported a series of mononuclear organometallic Pd(III) complexes stabilized by tetradentate ^RN₄ ligands (^RN₄ = *N,N'*-dialkyl-2,11-diaza[3.3]-(2,6)pyridinophane, R = *t*Bu, *i*Pr, Me)^{22,23} and studied their aerobic oxidation and C–C/C–heteroatom bond formation reactivity.^{24,25} In addition, we have shown that the tridentate ligand *N',N'',N'''*-trimethyltriazacyclononane (Me₃tacn) can stabilize halogen-bridged dinuclear Pd^{III} complexes that are active catalysts for the Kharasch radical addition.²⁶ These results suggest that Pd(III) complexes are more common than previously anticipated, and thus it prompted us to synthesize and characterize Pd(III) species supported by various ligand systems. In this regard, we have recently employed the N- and S-donor tetradentate ligand N2S2 (N2S2 = 2,11-dithia[3.3](2,6)-pyridinophane) and investigated the oxidatively induced methyl

group transfer reactivity of the dinuclear species [(N2S2)-Pd^{III}Me]₂(OTf)₂ (**5**).²⁷ Reported herein are the synthesis, characterization, and reactivity studies of a series of organometallic (N2S2)PdRX complexes (Scheme 1) that can promote C–C or C–Cl/Br bond formation reactions. These reactions

Scheme 1. (N2S2)Pd^{II}RX Complexes



Received: April 5, 2013

Published: May 29, 2013

involve both Pd(III) and Pd(IV) intermediates, as suggested by spectroscopic, electrochemical, and mechanistic studies.

EXPERIMENTAL SECTION

Reagents and Materials. All manipulations were carried out under a nitrogen atmosphere using standard Schlenk and glovebox techniques, if not indicated otherwise. All chemicals were commercially available from Aldrich, Fisher, or Strem Chemicals and were used as received without further purification. Acetylferrocenium tetrafluoroborate ($[\text{AcFc}^+]\text{BF}_4^-$),²⁸ (COD)Pd^{II}Me₂,²⁹ (COD)Pd^{II}(CD₃)₂,²⁴ (COD)-Pd^{II}MeCl,³⁰ (N2S2)Pd^{II}Cl₂ (**4**),³¹ and [(N2S2)Pd^{II}Me]₂(OTf)₂ (**5**)²⁷ were prepared according to the literature procedures. Solvents were purified prior to use by passing through a column of activated alumina using an MBraun solvent purification system. On the basis of their redox potential,²⁸ ferrocenium hexafluorophosphate ($[\text{Fc}^+]\text{PF}_6^-$), acetylferrocenium tetrafluoroborate ($[\text{AcFc}^+]\text{BF}_4^-$), and nitrosonium tetrafluoroborate ($[\text{NO}^+]\text{BF}_4^-$) were used as chemical oxidants for the oxidation of **1**, **2/3**, and **4**, respectively, while cobaltocene (Co^{II}Cp₂) was used as a reducing agent for the reduction of **1**²⁺.

Physical Measurements. ¹H (300.121 MHz) NMR spectra were recorded on a Varian Mercury-300 spectrometer. Low-temperature (−20 °C) ¹H (600 MHz) NMR spectra were recorded on a Varian Unity Inova-600 spectrometer. Chemical shifts are reported in ppm and referenced to residual solvent resonance peaks. Abbreviations for the multiplicity of NMR signals are s (singlet), d (doublet), t (triplet), q (quartet), sep (septet), m (multiplet), and br (broad). UV–vis spectra were recorded on a Varian Cary 50 Bio spectrophotometer. EPR spectra were recorded on a JEOL JES-FA X-band (9.2 GHz) EPR spectrometer in 1/3 MeCN/PrCN (v/v) at 77 K. Simulations of EPR spectra were performed using WinEPR SimFonia v. 1.25. Elemental analyses were carried out by the Columbia Analytical Services Tucson Laboratory. ESI-MS experiments were performed on a Bruker Maxis QTOF mass spectrometer with an electron spray ionization source. ESI mass spectrometry was provided by the Washington University Mass Spectrometry Resource, an NIH Research Resource (Grant No. P41RR0954).

Electrochemical Measurements. Electrochemical grade Bu₄NClO₄ or Bu₄NBF₄ from Aldrich was used as the supporting electrolyte. Cyclic voltammetry was performed with a BASi EC Epsilon electrochemical workstation or a CHI 660D Electrochemical Analyzer. Electrochemical measurements were carried out under a flow of nitrogen, and the analyzed solutions were deaerated by purging with nitrogen. A glassy-carbon electrode (GCE, *d* = 1 mm) was used as the working electrode, while a Pt wire was used as the auxiliary electrode. The nonaqueous reference electrode containing Ag/0.01 M AgNO₃ in 0.1 M Bu₄NClO₄/MeCN was calibrated against Fc; the potential of the Fc⁺/Fc couple vs the Ag/0.01 M AgNO₃/0.1 M Bu₄NClO₄/MeCN reference electrode is +0.105 V.

Synthesis of 2,11-Dithia[3.3](2,6)pyridinophane (N2S2). N2S2 was synthesized by following the reported procedure.^{31,32} The final product was first extracted in MeOH before being recrystallized out of toluene.

Synthesis of (N2S2)Pd^{II}Me₂ (1). (COD)Pd^{II}Me₂ was freshly made²⁹ and used immediately after preparation. Solid samples of (COD)Pd^{II}Me₂ (100 mg, 0.41 mmol) and N2S2 (112 mg, 0.41 mmol) were combined in 150 mL of anhydrous diethyl ether, and the reaction mixture was stirred at 0 °C for 3 h and then at 20 °C for 0.5 h. The white precipitate of (N2S2)Pd^{II}Me₂ was vacuum-filtered and washed with diethyl ether and pentane to give 111.9 mg for fraction 1. The filtrate was rotary-evaporated at 0 °C to give a pale yellow solid, which was suspended in 5 mL of anhydrous diethyl ether, vacuum-filtered, and washed with ether and pentane to give 38.8 mg for fraction 2. Total yield: 150.7 mg, 90%. ¹H NMR (acetone-*d*₆, 300 MHz; δ (ppm)): −0.027 (s, 6H, Me), 4.20 (d, *J* = 14.1 Hz, 4H, CH₂), 6.05 (d, *J* = 13.8 Hz, 4H, CH₂), 7.24 (d, *J* = 7.8 Hz, 4H, Py H_{meta}), 7.65 (t, *J* = 7.8 Hz, 2H, Py H_{para}). UV–vis (acetone; λ , nm (ϵ , cm^{−1} M^{−1})): 361 (sh, 800). Anal. Found: C, 46.57; H, 5.62; N, 6.76. Calcd for C₁₆H₂₀N₂PdS₂: C, 46.77; H, 4.91; N, 6.82. ESI-MS (*m/z*): 394.9891, calcd for [(N2S2)Pd^{II}Me]⁺ 394.9868.

Synthesis of (N2S2)Pd^{II}(CD₃)₂ (1-*d*₆). (COD)Pd^{II}(CD₃)₂ was freshly made²⁴ and used immediately after preparation. Solid samples of (COD)Pd^{II}(CD₃)₂ (39.5 mg, 0.157 mmol) and N2S2 (43.0 mg, 0.157 mmol) were combined in 20 mL of anhydrous diethyl ether, and the reaction mixture was stirred at 0 °C for 3 h and then at 20 °C for 0.5 h. The white precipitate of (N2S2)Pd^{II}(CD₃)₂ was vacuum-filtered and washed with diethyl ether and pentane to give 24.0 mg for fraction 1. The filtrate was rotary-evaporated at 0 °C to give a pale yellow solid, which was suspended in 2 mL of anhydrous diethyl ether, vacuum-filtered, and washed with ether and pentane to give 23.1 mg for fraction 2. Yield: 47.1 mg, 72%. The ¹H NMR spectrum of the product is identical with that of **1** except for the missing singlet of the PdMe group at −0.027 ppm. ESI-MS (*m/z*): 398.0081, calcd for [(N2S2)Pd(CD₃)₂]⁺ 398.0056.

Synthesis of (N2S2)Pd^{II}(¹³CH₃)₂ (1-¹³C). (COD)Pd^{II}(¹³CH₃)₂ was prepared by following the same procedure as for the preparation of (COD)Pd^{II}Me₂,²⁹ except with ¹³CH₃I instead of MeI. Freshly made (COD)Pd^{II}(¹³CH₃)₂ (104.1 mg, 0.423 mmol) and N2S2 (116.1 mg, 0.423 mmol) were combined in 100 mL of anhydrous diethyl ether, and the reaction mixture was stirred at 0 °C for 3 h and then at 20 °C for 0.5 h. The white precipitate of (N2S2)Pd^{II}(¹³CH₃)₂ was vacuum-filtered and washed with diethyl ether and pentane to give 87.0 mg for fraction 1. The filtrate was rotary-evaporated at 0 °C to give a pale yellow solid, which was suspended in 5 mL of anhydrous diethyl ether, vacuum-filtered, and washed with ether and pentane to give 35.0 mg for fraction 2. Yield: 122 mg, 70%. ¹H NMR (acetone-*d*₆, 300 MHz; δ (ppm)): −0.028 (d, 6H, ¹³CH₃, *J*(¹³C–¹H) = 127.2 Hz), 4.20 (d, *J* = 14.1 Hz, 4H, CH₂), 6.05 (d, *J* = 13.8 Hz, 4H, CH₂), 7.25 (d, *J* = 7.5 Hz, 4H, Py H_{meta}), 7.65 (t, *J* = 7.5 Hz, 2H, Py H_{para}). ESI-MS (*m/z*): 395.9913, calcd for [(N2S2)Pd(¹³CH₃)₂]⁺ 395.9902.

Synthesis of [(N2S2)Pd^{IV}Me₂](PF₆)₂ ([¹²⁺](PF₆)₂). A suspension of **1** (20.0 mg, 48.9 μ mol) in anhydrous acetone (3 mL) was added dropwise to a stirred solution of 2 equiv of FcPF₆ (32.4 mg, 97.8 μ mol) in anhydrous acetone (3 mL). After 1 h, the solution was set up for crystallization by diethyl ether diffusion. Light brown crystals formed after 1 day. Yield: 23.1 mg, 67%. ¹H NMR (acetone-*d*₆, 300 MHz; δ (ppm)): 2.61 (s, 6H, Me), 5.67 (d, *J* = 18 Hz, 4H, CH₂), 5.97 (d, *J* = 18 Hz, 4H, CH₂), 7.80 (d, *J* = 7.5 Hz, 4H, Py H_{meta}), 8.11 (t, *J* = 7.5 Hz, 2H, Py H_{para}). UV–vis (MeCN; λ , nm (ϵ , cm^{−1} M^{−1})): 318 (4000). Anal. Found: C, 30.21; H, 3.37; N, 3.74. Calcd for C₁₆H₂₀N₂PdS₂P₂F₁₂·CH₃COCH₃: C, 30.07; H, 3.45; N, 3.69. ESI-MS (*m/z*): 205.0063, calcd for [(N2S2)Pd^{IV}Me₂]²⁺ 205.0051.

Synthesis of (N2S2)Pd^{II}MeCl (2). N2S2 (85.0 mg, 0.310 mmol) and (COD)Pd^{II}MeCl³⁰ (82.4 mg, 0.310 mmol) were stirred in 50 mL of anhydrous diethyl ether for 1 day. The yellow precipitate was filtered off, washed with 10–20 mL of anhydrous diethyl ether and 2–3 mL of pentane, and dried under vacuum. Yield: 105 mg, 79%. UV–vis (CH₂Cl₂; λ , nm (ϵ , cm^{−1} M^{−1})): 390 (sh, 700), 330 (sh, 1900). ¹H NMR (CDCl₃, 300 MHz; δ (ppm)): 0.79 (s, 3H, PdMe), 4.13 (d, *J* = 14 Hz, 2H, CH₂), 4.23 (d, *J* = 14 Hz, 2H, CH₂), 5.99 (d, *J* = 14 Hz, 2H, CH₂), 6.21 (d, *J* = 14 Hz, 2H, CH₂), 7.05 (d, *J* = 7 Hz, 2H, Py H_{meta}), 7.16 (d, *J* = 7 Hz, 2H, Py H_{meta}), 7.51 (t, *J* = 7 Hz, 1H, Py H_{para}), 7.60 (t, *J* = 7 Hz, 1H, Py H_{para}). Anal. Found: C, 40.61; H, 3.85; N, 6.11. Calcd for C₁₅H₁₇ClN₂PdS₂·0.5H₂O: C, 40.92; H, 4.12; N, 6.36. ESI-MS (*m/z*): 394.9897, calcd for [(N2S2)Pd^{II}Me]⁺ 394.9868; 414.9341, calcd for [(N2S2)Pd^{II}Cl]⁺ 414.9322.

Synthesis of (N2S2)Pd^{II}MeBr (3). Acetyl bromide (5.9 μ L, 78.0 μ mol, 1.0 equiv) was added to a solution of **1** (31.9 mg, 78.0 μ mol) in 3 mL of anhydrous CH₂Cl₂. The reaction mixture was stirred at room temperature for 6 h. The resulting pale yellow precipitate was filtered off, washed with 2 mL of ether and 2 mL of pentane, and dried under vacuum. Recrystallization was performed in CH₂Cl₂ solution by diethyl ether diffusion. Yellow-orange crystals formed after 1–2 days at room temperature. Yield: 21.4 mg, 58%. ¹H NMR (acetone-*d*₆, 300 MHz; δ (ppm)): 0.64 (s, 3H, PdMe), 4.28 (d, *J* = 15 Hz, 2H, CH₂), 4.49 (d, *J* = 14 Hz, 2H, CH₂), 5.87 (d, *J* = 14 Hz, 2H, CH₂), 6.14 (d, *J* = 14 Hz, 2H, CH₂), 7.28 (d, *J* = 7 Hz, 2H, Py H_{meta}), 7.44 (d, *J* = 7 Hz, 2H, Py H_{meta}), 7.69 (t, *J* = 7 Hz, 1H, Py H_{para}), 7.81 (t, *J* = 7 Hz, 1H, Py H_{para}). UV–vis (MeCN; λ , nm (ϵ , cm^{−1} M^{−1})): 368 (sh, 980). ESI-MS (*m/z*): 394.9891, calcd for [(N2S2)Pd^{II}Me]⁺: 394.9868; 460.8806, calcd for

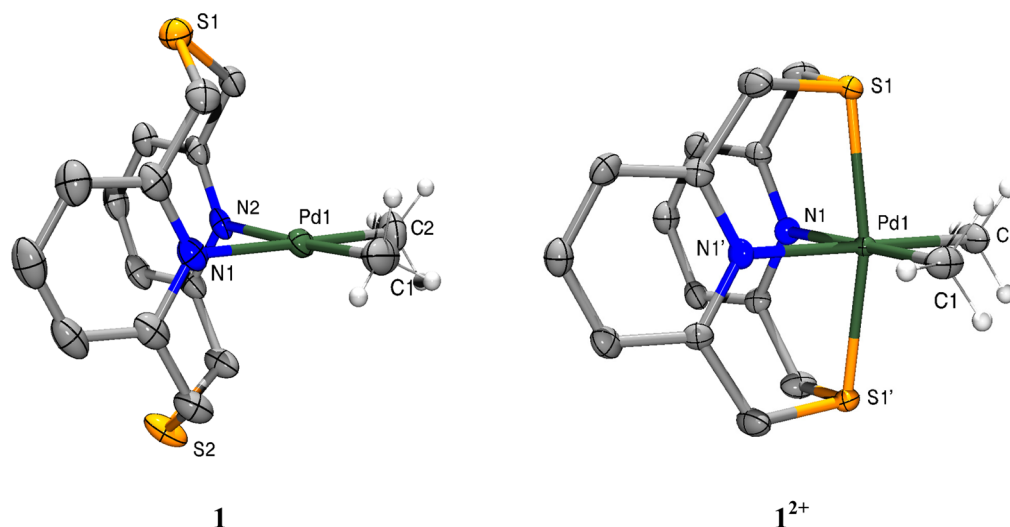


Figure 1. X-ray crystal structures of **1** and **1**²⁺ with 50% thermal ellipsoids. Selected bond distances (Å): **1**, Pd1–C1 = 2.043(5), Pd1–C2 = 2.035(4), Pd1–N1 = 2.184(3), Pd1–N2 = 2.194(3); **1**²⁺, Pd1–C1/C1' = 2.082(11), Pd1–N1/N1' = 2.151(8), Pd1–S1/S1' = 2.323(2).

[(N2S2)Pd^{II}Br]⁺ 460.8821. The (N2S2)Pd^{II}BrCl side product cocrystallized with **3** and was estimated to be present in 10–20% amount on the basis of ¹H NMR and 25% on the basis of the X-ray crystal structure. However, it is expected that (N2S2)Pd^{II}BrCl, by analogy to (N2S2)Pd^{II}Cl₂, has a Pd^{II/III} oxidation potential higher than that of **3**, and thus (N2S2)Pd^{II}BrCl should not be oxidized by AcFc⁺ and should not affect the oxidative reactivity of **3**.

Synthesis of (N2S2)Pd^{II}(¹³CH₃)Br (3**-¹³C).** Acetyl bromide (5.2 μL, 70.0 μmol, 1.0 equiv) was added to a solution of **1**-¹³C (28.8 mg, 70.0 μmol) in 3 mL of anhydrous CH₂Cl₂. The resulting pale yellow precipitate was filtered off, washed with 2 mL of ether and 2 mL of pentane, and dried under vacuum. Recrystallization was performed in CH₂Cl₂ solution by diethyl ether diffusion. Yellow-orange crystals formed after 1–2 days at room temperature. Yield: 20.9 mg, 63%. ¹H NMR (acetone-*d*₆, 300 MHz; δ (ppm)): 0.64 (d, 3H, ¹³CH₃, J(¹³C–¹H) = 134.4 Hz), 4.28 (d, J = 15 Hz, 2H, CH₂), 4.49 (d, J = 14 Hz, 2H, CH₂), 5.87 (d, J = 14 Hz, 2H, CH₂), 6.14 (d, J = 14 Hz, 2H, CH₂), 7.28 (d, J = 7 Hz, 2H, Py H_{meta}), 7.44 (d, J = 7 Hz, 2H, Py H_{meta}), 7.69 (t, J = 7 Hz, 1H, Py H_{para}), 7.81 (t, J = 7 Hz, 1H, Py H_{para}). ESI-MS (*m/z*): 395.9914, calcd for [(N2S2)Pd(¹³CH₃)]⁺ 395.9902; 460.8815, calcd for [(N2S2)-Pd^{II}Br]⁺ 460.8821.

Synthesis of [(N2S2)Pd^{II}Cl](OTf) (6**).** A solution of AgOTf (17.6 mg, 68.4 μmol) in MeCN (1 mL) was added to a stirred solution of **4** (30.9 mg, 68.4 μmol) in MeCN (10 mL). A white precipitate of AgCl appeared immediately, and the solution changed from yellow to brown. After the mixture was stirred at room temperature for 2 h in the dark, the solvent was removed by rotary evaporation. The solid residue was redissolved in a minimum amount of MeCN, and the resulting brown solution was filtered through Celite. A clear dark red filtrate was set to crystallize by anhydrous diethyl ether vapor diffusion at room temperature. Dark red crystals formed after several days. Yield: 18.0 mg, 47%. ¹H NMR (CD₃CN, 300 MHz; δ (ppm)): 4.38 (d, J = 16.2 Hz, 4H, CH₂), 4.93 (d, J = 16.5 Hz, 4H, CH₂), 7.14 (d, J = 7.8 Hz, 4H, Py H_{meta}), 7.50 (t, J = 7.8 Hz, 2H, Py H_{para}). UV–vis (MeCN; λ, nm (ε, cm⁻¹ M⁻¹)): 422 (2500), 341 (4100). Anal. Found: C, 31.95; H, 2.75; N, 4.98. Calcd for C₁₅H₁₄ClF₃N₂O₃PdS₃: C, 31.87; H, 2.50; N, 4.96. ESI-MS (*m/z*): 414.9335, calcd for [(N2S2)Pd^{II}Cl]⁺ 414.9322.

EPR Studies of the Formation of Pd(III) Intermediates. An EPR tube was charged with a solution of Pd complex in 1/3 MeCN/PrCN (v/v) and immersed into liquid nitrogen. Another solution containing 1 equiv of chemical oxidant or reductant in the same solvent mixture was quickly added and frozen as a second layer in the EPR tube. An initial EPR spectrum was taken at 77 K. The sample was then carefully warmed for 10–30 s to allow the two layers to mix and quickly refrozen, and the EPR spectrum was recorded. The warming step was repeated if necessary.

ESI-MS Studies of the Formation of Pd(III) Intermediates. All solutions were precooled to –40 °C. To a solution of Pd complex in 1 mL of MeCN was added a solution of 1 equiv of chemical oxidant at –40 °C. The mixture was thoroughly mixed and diluted to the required concentration for ESI-MS, followed by immediate injection into the instrument.

UV–Vis Study of the Formation of the [(N2S2)Pd^{III}Cl₂]⁺ (4**⁺) Complex.** A 3 mL solution of **4** (0.74 mM) in MeCN was mixed with an MeCN solution of 1 equiv of NOBF₄ in a quartz cuvette (10 mm path length) equipped with a septum-sealed cap. UV–vis spectra were recorded immediately after thorough mixing. However, the attempted isolation of **4**⁺ in the formation of a product mixture included the sulfoxide complex (N2S2-O)Pd^{II}Cl₂ (**7**), characterized by ¹H NMR (CD₃CN, 300 MHz; δ (ppm)): 4.49 (d, J = 15.0 Hz, 2H, CH₂), 5.05 (d, J = 14.1 Hz, 2H, CH₂), 6.27 (d, J = 15.0 Hz, 2H, CH₂), 6.48 (d, J = 14.1 Hz, 2H, CH₂), 7.15 (d, J = 7.5 Hz, 2H, Py H_{meta}), 7.41 (d, J = 7.5 Hz, 2H, Py H_{meta}), 7.74 (t, J = 7.8 Hz, 2H, Py H_{para}).

Low-Temperature Controlled-Potential Electrolysis (CPE) of **4 and in Situ Cyclic Voltammetry (CV).** Low-temperature (–40 °C) electrochemical oxidation was performed in a two-compartment H-shaped bulk electrolysis cell with a medium-frit glass junction and equipped with two septa and a magnetic stirring bar. Reticulated vitreous carbon was used as the working electrode for electrolysis, while a platinum wire was used as the working electrode for CV. Platinum gauze (25 mm × 10 mm) and a Ag/AgCl wire were used as the auxiliary electrode and the pseudo reference electrode, respectively. Electrochemical oxidation was performed at a constant potential at –40 °C under a blanket of nitrogen, and CVs were recorded before and after electrolysis.

General Procedure for NMR Studies of Reactivity of Pd Complexes upon Chemical Oxidation or Reduction. An NMR tube capped with a rubber septum was charged with a solution of Pd complex in 1.0 mL of acetone-*d*₆. A solution of 1 equiv of chemical oxidant or reductant in 1.4 mL of acetone-*d*₆ was added in portions with a microsyringe, and the mixture was thoroughly mixed after each addition. The yield of products was determined by NMR integration using dioxane as an internal standard, calculated as [moles of product]/[moles of starting complex] × 100% and reported as the average of two runs. Pd products were assigned on the basis of a comparison of the ¹H NMR spectra to those of independently synthesized complexes. For crossover experiments, a 1/1 mixture of nonlabeled and labeled complexes was used.

X-ray Structure Determination of **1, [**1**²⁺](PF₆)₂, and **6**.** Crystals of X-ray diffraction quality were obtained by anhydrous diethyl ether vapor diffusion into a CH₂Cl₂ solution for **1**, an acetone solution for [**1**²⁺](PF₆)₂, and an MeCN solution for **6**. Preliminary examination and

data collection were performed using a Bruker Kappa Apex-II Charge Coupled Device (CCD) Detector single-crystal X-ray diffractometer equipped with an Oxford Cryostream LT device. Data were collected using graphite-monochromated Mo $K\alpha$ radiation ($\lambda = 0.71073 \text{ \AA}$) from a fine focus sealed tube X-ray source. Apex II and SAINT software packages³³ were used for data collection and data integration. Data were corrected for systematic errors using SADABS on the basis of the Laue symmetry using equivalent reflections.³³ Structure solutions and refinement were carried out using the SHELXTL-PLUS software package.³⁴ Complete listings of geometrical parameters, positional and isotropic displacement coefficients for hydrogen atoms, and anisotropic displacement coefficients for the non-hydrogen atoms are available as Supporting Information.³⁵

RESULTS AND DISCUSSION

Synthesis and Characterization of (N2S2)Pd Complexes. X-ray Crystal Structures of (N2S2)Pd Complexes.

The (N2S2)Pd^{II}RX complexes (R = X = Me, **1**; R = Me, X = Cl, **2**; R = Me, X = Br, **3**; R = X = Cl, **4**; Scheme 1) were synthesized using common Pd(II) precursors and synthetic procedures.^{27,31,32} The X-ray crystal structure of (N2S2)Pd^{II}Me₂ (**1**; Figure 1) reveals a square-planar coordination at the Pd(II) center, with cis-positioned methyl groups and the two N donors from N2S2, in line with the typical κ^2 conformation of pyridinophane ligands in Pd(II) complexes.^{23,31,36} The average Pd–C and Pd–N bond lengths are 2.039 and 2.189 Å, respectively, consistent with the reported value of the (tmeda)-Pd^{II}Me₂ complex,³⁶ but with Pd–N distances significantly longer than those of **4** (Pd–N = 2.049 Å, Pd–Cl = 2.289 Å),³¹ likely due to the stronger trans influence of the Me vs Cl ligands.³⁷ Though no crystal structure was obtained for (N2S2)Pd^{II}MeCl (**2**), the preliminary crystal structure of (N2S2)Pd^{II}MeBr (**3**) reveals a square-planar geometry and the atom connectivity around the Pd(II) center, with N2S2 binding in a κ^2 conformation as in **1**.³⁵

Interestingly, chemical oxidation of **1** with 2 equiv of FcPF₆ in acetone yields a brown product that could be crystallized by ether vapor diffusion. X-ray structure analysis reveals a Pd(IV) complex, [(N2S2)Pd^{IV}Me₂](PF₆)₂ (**1**²⁺(PF₆)₂; Figure 1), with pseudo-octahedral geometry at the Pd center, which interacts with two N atoms and two S atoms of N2S2 (that adopts a κ^4 conformation) as well as with two cis-positioned methyl groups. The relatively longer Pd–C (2.082 Å) and shorter Pd–N bond distances (2.151 Å), in comparison to those of **1**, are likely a result of the oxidation of Pd(II) to Pd(IV), which favors an octahedral geometry, while the Pd–S bond lengths (2.323 Å) are similar to those for other reported systems.³⁸ Surprisingly, the presence of soft S donors can stabilize a high-valent Pd(IV) center. While there are Pd(II) and even Pd(III) complexes stabilized by thioether ligands,¹⁹ **1**²⁺ is to the best of our knowledge only the second Pd(IV) complex with thioether donors.³⁹ In addition, very few Pd(IV)–thiolate or –sulfonate complexes have been reported.^{40,41} On the basis of our recent studies on a series of (^RN4)Pd complexes (^RN4 = N,N'-dialkyl-2,11-diaza[3.3](2,6)pyridinophane, R = *t*Bu, *i*Pr, Me) containing Pd(II), Pd(III), and Pd(IV) oxidation states,²³ we propose that the ligand steric effects control the stability of Pd(III) vs Pd(IV) complexes (vide infra).²¹ The isolation of **1**²⁺(PF₆)₂ provides further evidence for the paramount role of ligand steric effects vs electronic effects, as the N2S2 ligand can accommodate the octahedral geometry of the Pd(IV) center, similar to the case for ^{Me}N4 and in contrast to the case for the bulkier ^{*i*Pr}N4 and ^{*t*Bu}N4 ligands that disfavor the stabilization of the Pd(IV) oxidation state.²³

Electrochemical Studies. The electrochemical properties of (N2S2)Pd^{II} complexes were studied by cyclic voltammetry (CV, Table 1). Complex **1** exhibits a complicated CV, and no Pd^{III/II}

Table 1. Cyclic Voltammetry (CV) Data for (N2S2)Pd Complexes^a

Complex	$E_{pa}^{II/III}$ (V)	$E_{pc}^{III/II}$ (V)	$E_{pa}^{III/IV}$ (V)	$E_{pc}^{IV/III}$ (V)
1 ^b		−0.4–0.27 (broad)		
1 ²⁺	<i>c</i>	−0.93	−0.56 ($\Delta E_p = 70 \text{ mV}$) ^d	
2	0.23	<i>c</i>	0.78	0.62
3 ^e	0.15	−0.21	0.80	0.58
4	~0.65	0.48	0.75 ($\Delta E_p = 70 \text{ mV}$) ^d	
5	0.55	0.09		0.88
6-Cl	0.81	0.61	<i>c</i>	<i>c</i>

^aReported vs Fc at room temperature. The scan rate was 100 mV/s, if not specified. ^b500 mV/s scan rate. ^cNot observed. ^dReversible. ^e50 mV/s scan rate.

redox wave could be identified, except some oxidation peaks that have potentials of $E_{pa} = 0.47 \text{ V}$ (vs Fc) and $E_{1/2} = -0.60 \text{ V}$ ($\Delta E_p = 70 \text{ mV}$) (Figure S1, Supporting Information), similar to the Pd^{III/II} oxidation potential of [(N2S2)Pd^{II}Me]₂(OTf)₂ (**5**; Figure S2, Supporting Information) and the Pd^{III/IV} redox potential of **1**²⁺ (Figure S3, Supporting Information), respectively. It is likely that the broad oxidation feature from −0.4 to 0.27 V is due to multiple oxidations such as Pd(II) → Pd(III) → Pd(IV), while the transiently formed Pd(III)–dimethyl intermediate can undergo a chemical reaction to yield a Pd(II)–monomethyl species on the CV time scale (vide infra). Interestingly, after one CV cycle a reversible redox wave is observed at ~−0.56 V, which is assigned to a Pd^{IV/III} redox couple, as it is similar to that observed during the reduction of **1**²⁺ (Figure S3). The CV of **1**²⁺ also suggests that the Pd(III)–dimethyl intermediate can be stabilized upon reduction of **1**²⁺, yet further reduction to Pd(II) leads to a decreased intensity for the reoxidations of Pd(II) to Pd(III) and Pd(III) to Pd(IV).³⁵ The observed limited stability of the Pd(III) intermediate is likely due to the conformational change of the N2S2 ligand. The oxidation of **1**, with N2S2 binding in a κ^2 conformation, generates a transient Pd(III) species with a four- or five-coordinate metal center that is expected to be less stable than a six-coordinate species. In contrast, N2S2 adopts a κ^4 conformation in **1**²⁺ and thus no conformation change is needed upon reduction to generate a (κ^4 -N2S2)Pd^{III} species. If Pd(III) is further reduced to Pd(II), the conformation change of N2S2 from κ^4 to κ^2 will lead to an irreversible reoxidation to Pd(III).

For **2** and **3**, both complexes display similar irreversible Pd^{III/II} and quasi-reversible Pd^{III/IV} waves (Table 1 and Figure S4 and S5 (Supporting Information)), indicating that the change in halogen donors (Cl, Br) does not affect significantly the electrochemical properties of the complexes. The additional features in the CVs of **2** and **3** are likely due to side reactions of the Pd(III) species to generate monohalide or monomethyl Pd(II) products that exhibit high potential oxidation waves (e.g., [(N2S2)Pd^{II}Cl]-(OTf) (**6-Cl**), Figure S8 (Supporting Information)).³⁵ The CV of **4** shows an irreversible Pd^{II/III} wave at a potential much higher than for any complex of **1**–**3**, which is due to the decreased σ -donor ability of a Cl vs methyl donor (Figure S6 (Supporting Information)). These CVs suggest that, while the Pd(III) oxidation state is accessible, it exhibits further reactivity on the CV time scale and the formed side products lead to complex CV profiles.

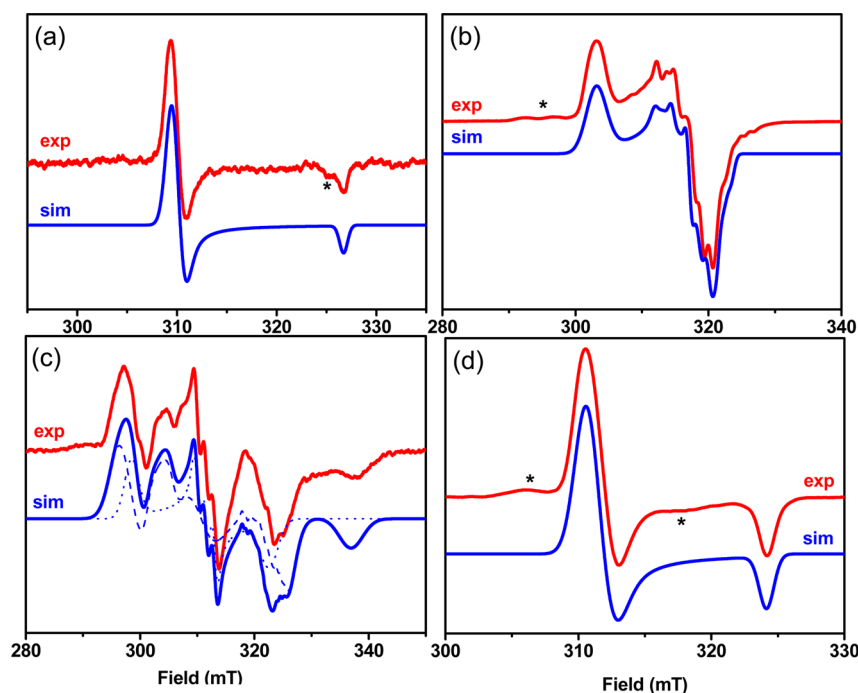


Figure 2. Experimental and simulated EPR spectra of reaction mixtures of (N2S2)Pd complexes and redox reagents at 77 K: (a) 1^+ + $\text{Co}^{\text{II}}\text{Cp}_2$ (the feature marked with an asterisk is from $\text{Co}^{\text{II}}\text{Cp}_2$); (b) 2 + AcFc^+ (the feature marked with an asterisk is from the hyperfine coupling to the ^{105}Pd isotope (abundance 22.3%, $I = 5/2$)); (c) 3 + AcFc^+ (the simulated spectrum (blue) is a sum of the components of two Pd(III) species: 3^+ (blue dashed line) and species B (blue dotted line)); (d) 4 + NO^+ (the features marked with an asterisk are due to the hyperfine coupling to the ^{105}Pd isotope (22.3%, $I = 5/2$)).

Table 2. EPR Parameters for Pd(III) Species

species	g value			Superhyperfine Coupling (G)		
	g_1	g_2	g_3	A_1	A_2	A_3
1^+	2.097	2.097	1.988			
2^+	2.143	2.045	2.038	ND ^a	$A_{\text{Cl}} = 25.0$ $A_{\text{N1}} = 5.0$ $A_{\text{N2}} = 13.0$	$A_{\text{N1}} = 15.0$
3 + AcFc^+						
species A	2.135	2.048	2.020	$A_{\text{N1}} = 15.0$	$A_{\text{Br}} = 130.0$ $A_{\text{N1}} = 5.0$ $A_{\text{N2}} = 5.0$	$A_{\text{N2}} = 30.0$
species B	2.177	2.086	2.014	ND ^a	$A_{\text{N}} = 15.0$	$A_{\text{N}} = 5.0$
4^+	2.093	2.084	2.005			

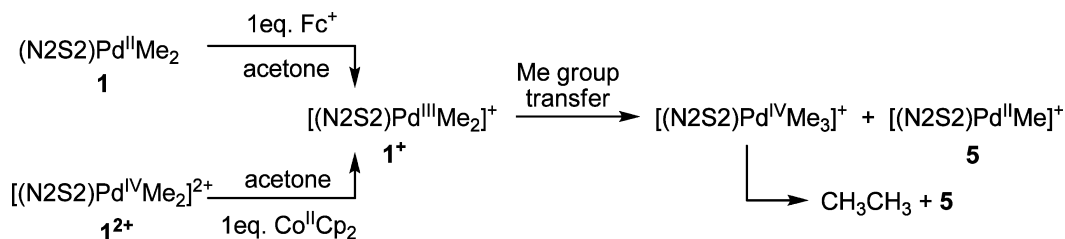
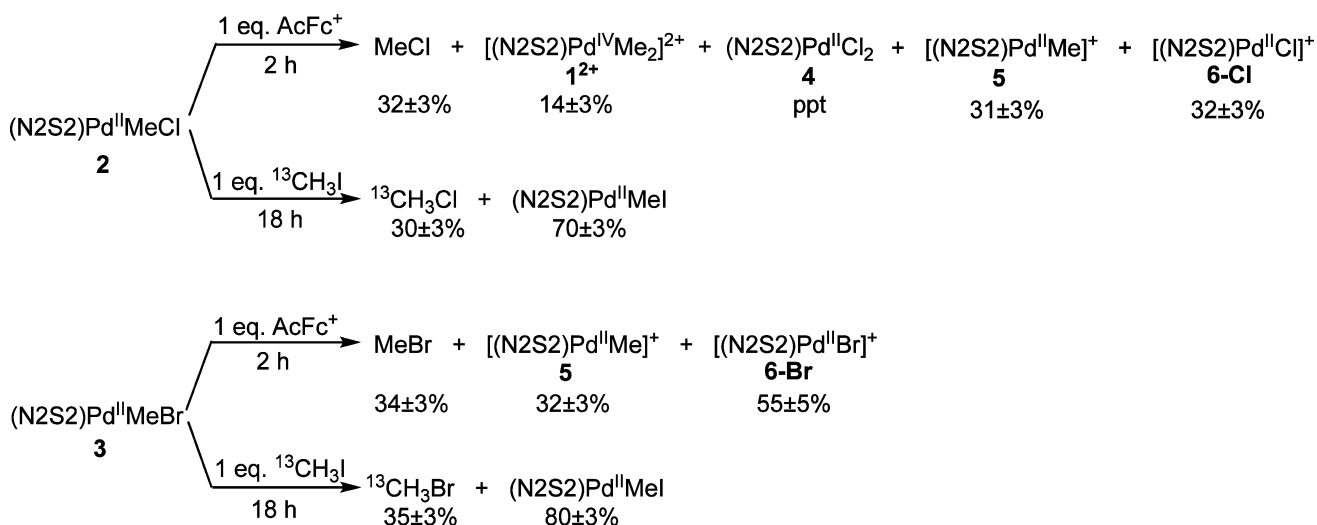
^aNot determined.

Characterization of Pd(III) Intermediates. On the basis of the CV studies of (N2S2)Pd complexes, controlled-potential electrolysis (CPE) was performed in an attempt to generate the corresponding Pd(III) intermediates. Unfortunately, the limited stability of the Pd(III) intermediates prevented their isolation. Instead, chemical oxidation or reduction was employed to generate Pd(III) species that were characterized in situ.

$[(\text{N2S2})\text{Pd}^{\text{III}}\text{Me}_2]^+$ (1^+). The formation of 1^+ upon adding 1 equiv of Fc^+ to 1 could not be detected by EPR. Alternatively, 1^+ was generated by chemical reduction of 1^{2+} with 1 equiv of $\text{Co}^{\text{II}}\text{Cp}_2$ and trapped by rapid freezing at 77 K. The EPR spectrum in 1/3 MeCN/PrCN (v/v) reveals an axial signal with $g_{\perp} = 2.097$ and $g_{\parallel} = 1.988$ (Figure 2), values similar to those reported for $[(^{\text{tBu}}\text{N4})\text{Pd}^{\text{III}}\text{Me}_2]^+$,²⁴ suggesting the presence of the Pd(III)–dimethyl intermediate in an axially distorted octahedral geometry. However, species 1^+ is highly unstable and decays within 1 min to generate EPR-silent species (vide infra).

$[(\text{N2S2})\text{Pd}^{\text{III}}\text{MeCl}]^+$ (2^+). 2^+ was made by oxidation of 2 with 1 equiv of AcFc^+ and trapped by rapid freezing at 77 K. The EPR spectrum in 1/3 MeCN/PrCN (v/v) is more complex (Figure 2), and a reasonable simulation was obtained using the parameters $g_1 = 2.143$, $g_2 = 2.045$ ($A_{\text{Cl}} = 25.0$ G, $A_{\text{N1}} = 5.0$ G, $A_{\text{N2}} = 13.0$ G), and $g_3 = 2.038$ ($A_{\text{N1}} = 15.0$ G) with superhyperfine coupling to one Cl atom (^{35}Cl , ^{37}Cl , $I = 3/2$) and two ^{14}N ($I = 1$) atoms. The similarity of these g values to the literature values implies that a Pd(III) intermediate has been produced.²² However, the $g_1 \gg g_2 \approx g_3$ ordering of the g values is different from that of most reported EPR spectra of mononuclear Pd(III) complexes in a distorted-octahedral geometry with a $(d_{z^2})^1$ ground state.²¹ This suggests that the Pd(III) center could adopt either a four-coordinate (square planar) or five-coordinate (trigonal pyramidal or square pyramidal) geometry and a $(d_{xy})^1$ or $(d_{x^2-y^2})^1$ ground state, although the geometry of the Pd(III) species cannot be unambiguously determined. The proposed geometries are also suggested by the observed superhyperfine

Scheme 3. Proposed Mechanism for C–C Bond Formation

Scheme 4. Oxidative Reactivity Studies of **2** and **3**^a^appt = precipitate.

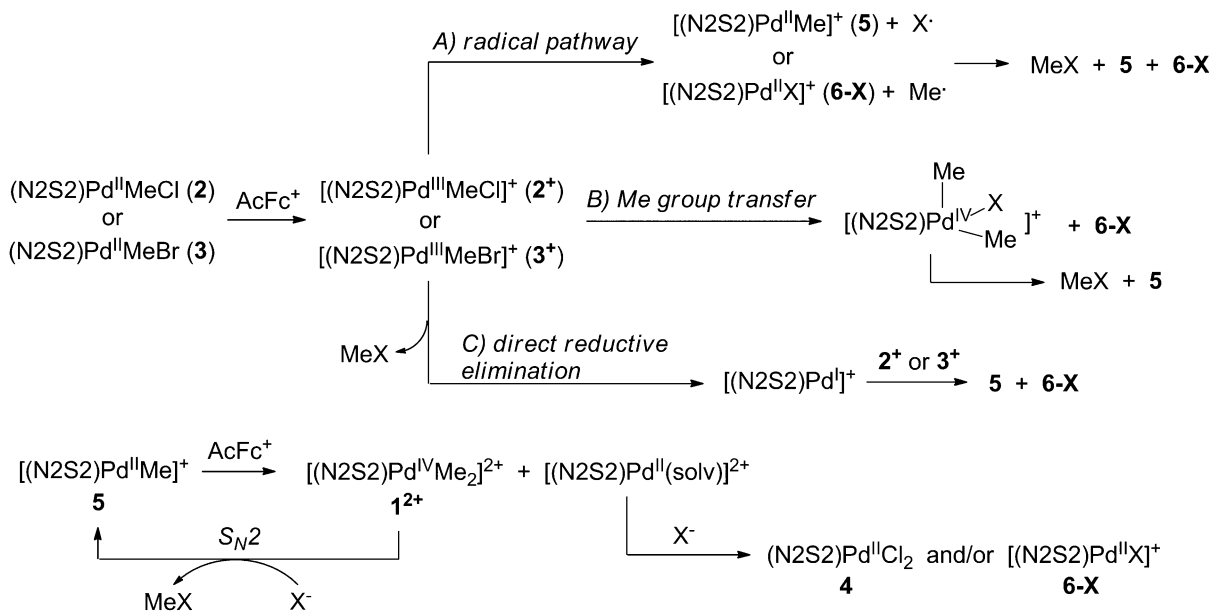
of a shoulder at 434 nm (Figure 3a). By comparing to other reported mononuclear Pd(III) complexes,^{22,42} we tentatively assign these bands to Cl to Pd and S to Pd ligand to metal charge transfer (LMCT) transitions for 4^+ , while the shoulder of 434 nm is likely an LMCT transition of the resulting product. Further insight into the electronic properties of 4^+ was obtained by density functional theory (DFT) calculations. The geometry optimized structure of 4^+ reveals a Pd(III) center in a distorted-octahedral geometry and the unpaired electron in a d_z^2 ground state, in line with the observed EPR spectrum.³⁵ In addition, the TD-DFT calculated UV–vis spectrum and transitions of 4^+ match well the experimental spectrum and proposed charge transfer transitions (Figure 3b and Table S4 (Supporting Information)) and thus provide strong support for the proposed octahedral geometry of 4^+ with the N2S2 ligand binding in a κ^4 conformation. Since the Pd(III) intermediate decays quickly at room temperature, low-temperature CPE of **4** (2.0 mM, 10 mL) was performed in MeCN at -40°C . After the charge equivalent to a one-electron oxidation has passed, the solution turns purple, indicating formation of 4^+ . In situ CV immediately after CPE at -40°C reveals a reversible Pd^{III/II} redox wave at 0.39 V, followed by another reduction at -0.11 V (Figure S6 (Supporting Information)).³⁵ Although the purple solution is stable at -35°C for a few days, the isolation of the purple product was not successful, an orange powder being obtained instead (vide infra).

Reactivity Studies of (N2S2)Pd Complexes. In light of the recently reported reductive elimination of ethane and MeCl from isolated Pd(III) complexes and the proposed role of Pd(III) intermediates in reductive elimination reactions,^{22,24,43} we set

out to investigate the oxidatively induced reactivity of organometallic (N2S2)Pd^{II} complexes **1**–**3**.

C–C Bond Formation. Oxidation of **1** with 1 equiv of Fc^+ in acetone- d_6 at room temperature leads to the quantitative formation of MeMe ($49 \pm 2\%$) and **5** ($98 \pm 1\%$) within 30 min (Scheme 2), as detected by NMR (Figure S12 (Supporting Information)).³⁵ In order to gain insight into the possible mechanism of ethane formation, we first examined the reaction of **1** with Fc^+ in the presence of 2 equiv of TEMPO, a common alkyl radical trapping agent, yet no Me-TEMPO product was observed and the yield of ethane was not affected. Along with the lack of formation of CH_4 , these results suggest that a methyl radical pathway is unlikely.²² Thus, we propose the initial formation of 1^+ , followed by methyl group transfer and disproportionation of 1^+ to $[(\text{N2S2})\text{Pd}^{\text{IV}}\text{Me}_3]^+$ and a mono-methyl Pd(II) product, the resulting $[(\text{N2S2})\text{Pd}^{\text{IV}}\text{Me}_3]^+$ species being responsible for the subsequent C–C bond formation (Scheme 3). A similar nonradical methyl group transfer and C–C bond formation reactivity was proposed by Sanford, Meyer, et al. for the one-electron oxidation of the $(^t\text{Bu}_2\text{bpy})\text{Pd}^{\text{II}}\text{Me}_2$ complex to generate an observable $[(^t\text{Bu}_2\text{bpy})\text{Pd}^{\text{IV}}\text{Me}_3]^+$ intermediate.^{43,44} In addition, the recent isolation of $[(\text{Me}_3\text{tacn})\text{Pd}^{\text{IV}}\text{Me}_3]^+$ and $[(^{\text{Me}}\text{N4})\text{Pd}^{\text{IV}}\text{Me}_3]^+$ species upon aerobic oxidation of the corresponding Pd(II) precursors and methyl group transfer at Pd(III) or Pd(IV) centers provides further support for the proposed mechanism (Scheme 3).^{13,25}

To further probe the mechanism of the reaction, a crossover experiment was performed using a 1/1 mixture of **1** and (N2S2)Pd^{II}(CD₃)₂ (**1**- d_6) in the presence of 2 equiv of Fc^+ (1 equiv Fc^+ per Pd), which leads to rapid formation of **5**,

Scheme 5. Possible Mechanisms for Reaction of **2** or **3** with AcFc^+ ($X = \text{Cl}, \text{Br}$)

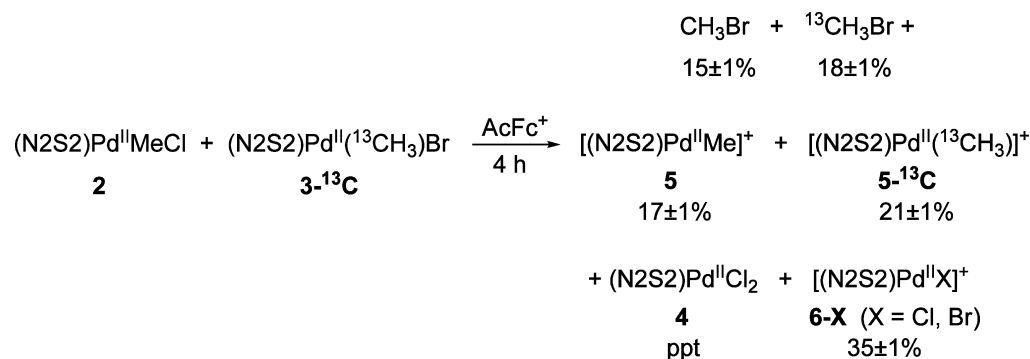
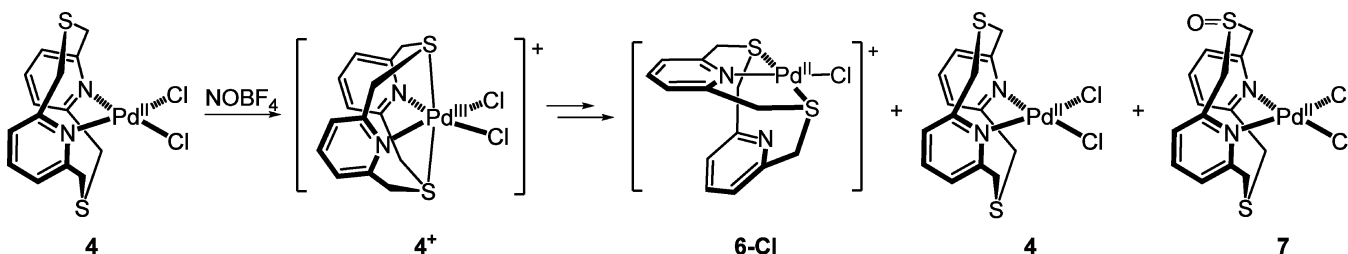
$(\text{N}2\text{S}2)\text{Pd}^{\text{II}}(\text{CD}_3)]^+$ (**5-d₃**), CH_3CH_3 , and CH_3CD_3 in 43 ± 9 , 57 ± 9 , 12 ± 2 , and $24 \pm 3\%$ yields, respectively (Figure S13 (Supporting Information)). Given the typical yield of $\sim 50\%$ ethane upon oxidation of **1**, the yield of CD_3CD_3 can be estimated as $\sim 14 \pm 6\%$, suggesting a $\sim 1/2/1$ ratio of CH_3CH_3 , CH_3CD_3 , and CD_3CD_3 . This ethane isotopologue ratio is similar to that observed for the one-electron oxidation of the $(^t\text{Bu}_2\text{bpy})\text{Pd}^{\text{II}}\text{Me}_2$ complex, further supporting the methyl group transfer mechanism.⁴³ Interestingly, this result is in contrast to a mechanism involving a rapid rearrangement of the methyl groups before reductive elimination, which should give a 1/1/1 ratio of CH_3CH_3 , CH_3CD_3 , and CD_3CD_3 , as observed for the aerobic oxidation of $(^R\text{N}4)\text{Pd}^{\text{II}}\text{Me}_2$ systems.^{24,25}

The involvement of Pd(IV) species during C–C bond formation is also suggested by the reaction of **1** with 10 equiv of MeI, which gives almost stoichiometric amounts of $(\text{N}2\text{S}2)\text{Pd}^{\text{II}}\text{MeI}$ and ethane in 70 h (Scheme 2 and Figure S14 (Supporting Information)), suggesting an oxidative addition step followed by ethane elimination. Moreover, the reaction of **1** with 10 equiv of CD_3I gives a less than 1/2 ratio of CH_3CH_3 and CH_3CD_3 and the corresponding monomethyl Pd(II) products (Figure S15 (Supporting Information)). Since a rapid reductive elimination step should lead to only CH_3CD_3 , the presence of both ethane isotopologues suggests that the transient Pd(IV) intermediate can undergo a rearrangement of the equatorial CH_3 and axial CD_3 groups before ethane elimination,²⁴ likely due to the reduced rate of reductive elimination from a six-coordinate $(\text{N}2\text{S}2)\text{Pd}^{\text{IV}}\text{Me}_2(\text{CD}_3)\text{I}$ transient species and in line with the observed longer reaction times (~ 70 h) for this reaction (Scheme 2).^{13,45,46}

Interestingly, no ethane formation was observed upon thermolysis or photolysis of an acetone solution of **1²⁺**, as expected for a rigid six-coordinate Pd(IV) species.²³ In contrast, the reduction of **1²⁺** by 1.1 equiv of $\text{Co}^{\text{II}}\text{Cp}_2$ can promote C–C bond formation and produces $38 \pm 1\%$ ethane and $80 \pm 6\%$ of **5** (Scheme 2, bottom),³⁵ confirming that the Pd(III)–dimethyl species **1⁺** is a key intermediate during the proposed ethane elimination mechanism.

C–X Bond Formation ($X = \text{Cl}, \text{Br}$). Oxidation of **2** by 1 equiv of AcFc^+ in acetone- d_6 generates $32 \pm 3\%$ MeCl within 2 h, as well as **1²⁺**, **5**, and $(\text{N}2\text{S}2)\text{Pd}^{\text{II}}\text{Cl}]^+$ (**6-Cl**) in $14 \pm 3\%$, $31 \pm 3\%$, and $32 \pm 3\%$ yields, respectively (Scheme 4, top). The reaction of **2** with 1 equiv of Fc^+ gives a similar result, yet it takes 8 h to reach completion.³⁵ In addition, formation of **4** was observed by ^1H NMR in the early stages of the reaction but disappeared at the completion of the reaction along with formation of a yellow precipitate identified as **4**. Since the Pd(III) intermediate **2⁺** was already observed by EPR and ESI-MS, several possible mechanisms were proposed for the observed reactivity: (a) a radical pathway, (b) a methyl group transfer/disproportionation step, and (c) direct reductive elimination from the Pd(III) species (Scheme 5). The formation of small amounts of **1²⁺** during the reaction is most likely due to the subsequent oxidation of the monomethyl Pd(II) product **5**, followed by methyl group transfer and disproportionation.²⁷

Addition of TEMPO during the oxidation reaction does not lead to formation of TEMPO-Me and does not affect the yield of MeCl, suggesting that a mechanism involving methyl radicals is unlikely. Monitoring of the reaction of **2** with AcFc^+ by ^1H NMR at -20°C reveals the formation of a significant amount of **5** ($\sim 60\%$ yield), followed by its decay and an increase of the amount of all products during the course of several hours (Figure S23a (Supporting Information)),³⁵ suggesting a possible Cl radical pathway. However, the absence of any Cl trapped products by using halogen radical trapping agents (2,3-dimethyl-1,3-butadiene, styrene, 1-hexene, etc.) in GC-MS or ^1H NMR makes the Cl radical pathway less likely.^{47–49} Moreover, the reaction of **2** with 1 equiv of $^{13}\text{CH}_3\text{I}$ produces only $^{13}\text{CH}_3\text{Cl}$ and $(\text{N}2\text{S}2)\text{Pd}^{\text{II}}\text{MeI}$ (Figure S18 (Supporting Information)), suggesting that the Pd(IV) oxidation state is accessible, a fast and selective reductive elimination of $^{13}\text{CH}_3\text{Cl}$ occurs from a $(\text{N}2\text{S}2)\text{Pd}^{\text{IV}}(^{13}\text{CH}_3)\text{MeCl}]^+$ intermediate, and no scrambling occurs between the axial and equatorial methyl groups due to the high reactivity of the transient Pd(IV) species. Overall, these results suggest a mechanism involving methyl group transfer and disproportionation to give a $(\text{N}2\text{S}2)\text{Pd}^{\text{IV}}\text{Me}_2\text{Cl}]^+$ species, followed by reductive elimination (Scheme 5, path B).

Scheme 6. Crossover Experiment between 2 and 3-¹³CScheme 7. Oxidation Reaction of 4 with 1 equiv of NOBF₄

By comparison, oxidation of 3 with 1 equiv of AcFc⁺ gives 34 ± 3% MeBr, 55 ± 5% [(N2S2)Pd^{IV}Br]⁺ (6-Br), and 32 ± 3% of 5, respectively (Scheme 4, bottom; Figure S19 (Supporting Information)), yet no I²⁺ or any precipitate was observed at the end of the reaction of 2 h. Moreover, the time-dependent low-temperature ¹H NMR studies of this reaction reveal a behavior different from that of 2. All products form with similar rates, while the amount of starting material decreases. While I²⁺ was generated at the beginning of the reaction, its concentration remained constant for several hours at -20 °C and then slowly decayed within 14 h at room temperature, along with an increase of all product yields. Overall, these results indicate that different mechanisms might be involved during the oxidative reactivity of 3.

A radical mechanism is also unlikely in this case, as no TEMPO-Me product was observed when the oxidation reaction was performed in the presence of TEMPO, and no Br-containing adducts were obtained in the presence of various alkenes (2,3-dimethyl-1,3-butadiene, 1-hexene, cyclohexene, styrene, etc.) as halogen radical traps.^{47–49} However, the possibility of Br radical cannot be excluded completely, due to a possible rapid reduction of the Br radical to the Br⁻ anion. Moreover, the intermediacy of I²⁺ leading to product formation suggests that I²⁺ could react with Br⁻ through an S_N2 mechanism to produce MeBr and 5 (Scheme 5, bottom). Indeed, this has been confirmed by reacting I²⁺ with 1.8 equiv of tetrabutylammonium bromide (Bu₄N⁺Br⁻), which eliminates MeBr and 3 within 5 min (Figure S22 (Supporting Information)). By comparison, the reaction of I²⁺ with 1.8 equiv of tetrabutylammonium chloride (Bu₄N⁺Cl⁻) produces MeCl at a much slower rate than a similar reaction with Bu₄N⁺Br⁻.

Similarly to 2, the reaction of 3 with 1 equiv of ¹³CH₃I produces only ¹³CH₃Br and (N2S2)Pd^{IV}MeI (Scheme 4, bottom, and Figure S20 (Supporting Information)), implying that [(N2S2)Pd^{IV}Me₂Br]⁺ could be a reaction intermediate (Scheme 5).³⁵ Overall, these mechanistic studies suggest that the oxidatively induced MeBr formation from 3 can occur by more

than one mechanism, involving either an initial methyl group transfer/disproportionation from a Pd(III) center followed by C–Br bond formation or an S_N2 reductive elimination from a Pd(IV)–dimethyl intermediate.

To test whether a direct reductive elimination from a Pd(III) center is involved during the oxidative reactivity of 2 and 3 (Scheme 5, path C), a crossover experiment was conducted by reacting a 1/1 mixture of 2 and (N2S2)Pd^{II}(¹³CH₃)Br (3-¹³C) with AcFc⁺. A concerted reductive elimination is expected to generate only the non-scrambled products MeCl and ¹³CH₃Br, respectively. However, the oxidation reactions generated CH₃Br, ¹³CH₃Br, 5, and [(N2S2)Pd^{IV}(¹³CH₃)]⁺ (5-¹³C) in a ~1/1/1/1 ratio, as well as 6-Cl/Br and a yellow precipitate corresponding to 4 (Scheme 6), while a negligible amount of MeCl (~1%) was produced after 4 h. The formation of the two isotopomers of MeBr argues against a concerted reductive elimination from a Pd(III) center and supports a methyl group transfer mechanism as the preferred pathway for C–Br bond formation. The different yields of MeCl and MeBr are proposed to be due to (a) the slightly higher oxidation potential (80 mV) of Pd^{II/III} of 2 vs that of 3 (although their oxidation by AcFc⁺ is rapid at room temperature, as observed by NMR),³⁵ (b) the differential reactivity of [(N2S2)Pd^{IV}Me₂Cl]⁺ and [(N2S2)Pd^{IV}Me₂Br]⁺ species toward concerted reductive elimination, (c) the more rapid reaction of Br⁻ vs Cl⁻ with I²⁺ to give MeBr through an S_N2 reductive elimination, or (d) a combination of the preceding.

On the basis of all these studies, we propose that the observed oxidatively induced C–halide bond formation from 2 or 3 most likely involves initial formation of Pd(III) species, followed by methyl group transfer and disproportionation to form [(N2S2)Pd^{IV}Me₂X]⁺ (X = Cl, Br) intermediates that selectively eliminate MeCl or MeBr. However, a halogen radical pathway, especially for 3, cannot be unambiguously excluded, yet such a radical mechanism can generate an appreciable amount of 5, which can be oxidized to yield I²⁺ that can undergo S_N2 reductive elimination with Br⁻ (or Cl⁻) to yield MeBr (and to a lesser extent MeCl). In addition, an S_N2 reductive elimination from a

$\text{Pd}^{\text{III}}\text{-Me}$ intermediate cannot be completely ruled out either, although such a reaction was not observed in any of our previous studies on organometallic Pd(III) systems.^{22–25}

Partial Ligand Oxidation of $[(\text{N}2\text{S}2)\text{Pd}^{\text{III}}\text{Cl}_2]^+$ (4^+). Characterization of the one-electron-oxidation product of **4** by EPR, low temperature UV–vis, and CV strongly suggests the formation of the red-purple Pd(III) species 4^+ (vide supra). Unfortunately, attempts to isolate pure 4^+ were unsuccessful and led to the formation of an orange solid. Diffusion of diethyl ether into an MeCN solution of the orange powder yielded orange crystals whose X-ray characterization reveals a unit cell that contains $[(\text{N}2\text{S}2)\text{Pd}^{\text{II}}\text{Cl}]^+$ (**6-Cl**) and $(\text{N}2\text{S}2)\text{Pd}^{\text{II}}\text{Cl}_2$ (**4**), along with a small amount of the new complex $(\text{N}2\text{S}2\text{-O})\text{Pd}^{\text{II}}\text{Cl}_2$ (**7**; Scheme 7), in which one of the S atoms of N2S2 has been oxidized to a sulfoxide (the sulfoxide O atom exhibits a 14% occupancy in the crystal structure).³⁵ The pure complex **[6-Cl](OTf)** was synthesized independently, and its X-ray structure reveals an uncommon κ^3 conformation for the N2S2 ligand, which binds to the Pd(II) center through one N and two S donors, and the chloride completes the square-planar geometry (Figure 4), in

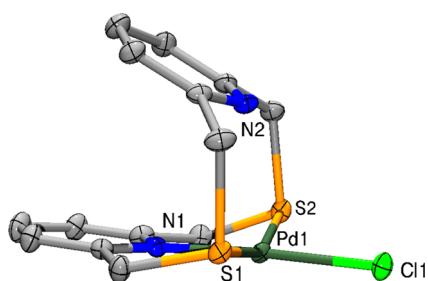


Figure 4. X-ray crystal structure of the cation of **[6-Cl](OTf)** with 50% thermal ellipsoids. Average bond distances (Å): Pd1–N1 = 2.030, Pd1–Cl1 = 2.292, Pd1–S1 = 2.319, Pd1–S2 = 2.328.

line with the atom connectivity obtained from the isolated orange mixture. A similar ligand conformation was observed for the recently reported dinuclear Pd(II) complexes $[(\text{N}2\text{S}2)\text{Pd}^{\text{II}}\text{Me}_2]^{2+}$ and $[(\text{N}2\text{S}2)\text{Pd}^{\text{II}}(\text{MeCN})]_2^{4+}$, yet no metal–metal interactions were observed for **[6-Cl](OTf)** in the solid state.²⁷ By comparison, the N2S2 ligand in **4** and **7** is found in the more common κ^2 conformation. The conformational change of N2S2

upon oxidation of Pd(II) to Pd(III) is proposed to lead to the partial ligand oxidation; however, detailed mechanistic studies are needed for a better understanding of this ligand oxidation reactivity.

Comparison of Electronic Properties of Analogous N2S2 and $^t\text{BuN}4$ Pd(III) Complexes. The results above show that the Pd(III) complexes supported by the N- and S-donor N2S2 ligand exhibit limited stability, although the Pd(IV) complex $[(\text{N}2\text{S}2)\text{Pd}^{\text{IV}}\text{Me}_2](\text{PF}_6)_2$ is uncommonly stable. By comparison, recent reports from our laboratory have shown that the analogous Pd(III) complexes of the all-N macrocyclic ligand $^t\text{BuN}4$ are extremely stable, although the corresponding Pd(IV) species could not be isolated.^{21,22,24} In order to address whether the differential stability of the Pd(III) complexes is due to the axial donor atom (N vs S) or just steric effects, density functional theory (DFT) calculations were employed to evaluate the electronic properties of the geometry optimized $\text{Pd}^{\text{III}}\text{Me}_2$ cationic complexes stabilized by N2S2 or $^t\text{BuN}4$, which most likely exhibit the same geometry of the Pd(III) centers. By comparison, the geometry of the Pd(III) centers in **2** and **3** is not clear at this point, either a five- or six-coordinate geometry being possible. Interestingly, the atomic contribution to the frontier molecular orbitals is similar for N2S2 vs $^t\text{BuN}4$ Pd(III) complexes (Table 3 and Tables S1–S6 (Supporting Information)), with the N2S2 complexes exhibiting slightly more covalent metal–ligand interactions and suggesting that the change in axial donors has only a minor effect. Thus, the steric effect of the N- ^tBu group is most likely responsible for the dramatic stabilization of the distorted-octahedral Pd(III) complexes, while the absence of such groups in the N2S2 ligand supports an octahedral geometry preferred by Pd(IV) complexes. Moreover, a similar steric effect was observed for the Pd complexes of $^R\text{N}4$ ligands (R = Me, $i\text{Pr}$),^{23,25} which can stabilize both Pd(III) and Pd(IV) oxidation states. Use of the N2S2 ligand thus further highlights the paramount role of ligand sterics on Pd(III) complex stability that seems to trump even the change in axial donor atoms.

CONCLUSION

In summary, reported herein is the characterization of a series of organometallic $(\text{N}2\text{S}2)\text{Pd}^{\text{II}}$ complexes that exhibit oxidatively induced ethane, MeCl, or MeBr elimination reactivity. We have

Table 3. Comparison of the β Lowest Unoccupied Molecular Orbitals (LUMOs) of $[(\text{N}2\text{S}2)\text{Pd}^{\text{III}}\text{Me}_2]^+$ and $[(^t\text{BuN}4)\text{Pd}^{\text{III}}\text{Me}_2]^+$ Complexes

$[(\text{N}2\text{S}2)\text{Pd}^{\text{III}}\text{Me}_2]^+$	$[(^t\text{BuN}4)\text{Pd}^{\text{III}}\text{Me}_2]^+$
<p>Pd 29% S 40% Me 18%</p>	<p>Pd 32% N_{ax} 32% Me 16%</p>

shown that the Pd(III) oxidation state is accessible on the basis of the redox properties of these complexes and that the oxidative reactivity of these Pd(II) complexes involves Pd(III) intermediates. EPR, UV–vis, ESI-MS, and low-temperature CV provide direct evidence for the presence of Pd(III) intermediates. Mechanistic studies suggest that C–C bond formation occurs most likely through a methyl group transfer and formation of a transient $[(N_2S_2)Pd^{IV}Me_3]^+$ intermediate. In contrast, C–halide bond formation may involve the formation of $[(N_2S_2)Pd^{IV}Me_2X]^+$ intermediates, yet a halogen radical pathway cannot be completely excluded. The isolated Pd^{IV}–dimethyl complex reveals a N₂S₂ ligand that adopts a tetradentate κ^4 conformation, while in the Pd^{II}–monochloro complex N₂S₂ adopts a tridentate κ^3 conformation, both showing that the S-donor atoms interact with the metal center in different oxidation states. Moreover, the Pd complexes described herein reveal the ability of the N₂S₂ ligand to adopt various conformations and denticities when binding to metal centers in various oxidation states and ligand field strengths. The coordination versatility of N₂S₂ is currently being explored for other transition-metal ions.

■ ASSOCIATED CONTENT

■ Supporting Information

Figures, tables, and CIF files giving cyclic voltammograms, ESI-MS spectra, EPR simulation details, ¹H NMR spectra, computational details, and X-ray crystallographic data. This material is available free of charge via the Internet at <http://pubs.acs.org>.

■ AUTHOR INFORMATION

Corresponding Author

*E-mail for L.M.M.: mirica@wustl.edu.

Notes

The authors declare no competing financial interest.

■ ACKNOWLEDGMENTS

We thank the Department of Chemistry at Washington University for startup funds and the DOE Catalysis Science Program (DE-FG02-11ER16254) for support. We also thank Dr. Julia R. Khusnutdinova for help with low-temperature electrochemical studies, Ying Zhang for ESI-MS analyses, Jason Schultz for EPR measurements, and Dr. Xia Ge for low-temperature ¹H NMR experiments.

■ REFERENCES

- (1) Diederich, F.; Stang, P. J. *Metal-Catalyzed Cross-Coupling Reactions*; Wiley-VCH: Weinheim, New York, 1998.
- (2) Lyons, T. W.; Sanford, M. S. *Chem. Rev.* **2010**, *110*, 1147.
- (3) Xu, L.-M.; Li, B.-J.; Yang, Z.; Shi, Z.-J. *Chem. Soc. Rev.* **2010**, *39*, 712.
- (4) Sehnal, P.; Taylor, R. J. K.; Fairlamb, I. J. S. *Chem. Rev.* **2010**, *110*, 824.
- (5) Henry, P. M. *Palladium Catalyzed Oxidation of Hydrocarbons*; D. Reidel: Boston, MA, 1980.
- (6) Negishi, E. *Handbook of Organopalladium Chemistry for Organic Synthesis*; Wiley: Hoboken, NJ, 2002.
- (7) van Leeuwen, P. W. N. M. *Homogeneous Catalysis: Understanding the Art*; Kluwer Academic: Dordrecht, The Netherlands, 2004.
- (8) Hartwig, J. F. *Organotransition Metal Chemistry: From Bonding to Catalysis*; University Science Books: Sausalito, CA, 2010.
- (9) Canty, A. J. *Dalton Trans.* **2009**, 10409.
- (10) Chen, X.; Engle, K. M.; Wang, D. H.; Yu, J. Q. *Angew. Chem., Int. Ed.* **2009**, *48*, 5094.
- (11) Muniz, K. *Angew. Chem., Int. Ed.* **2009**, *48*, 9412.
- (12) Powers, D. C.; Ritter, T. *Top. Organomet. Chem.* **2011**, *35*, 129.
- (13) Khusnutdinova, J. R.; Qu, F.; Zhang, Y.; Rath, N. P.; Mirica, L. M. *Organometallics* **2012**, *31*, 4627.
- (14) Chuang, G. J.; Wang, W.; Lee, E.; Ritter, T. *J. Am. Chem. Soc.* **2011**, *133*, 1760.
- (15) Powers, D. C.; Benitez, D.; Tkatchouk, E.; Goddard, W. A., III; Ritter, T. *J. Am. Chem. Soc.* **2010**, *132*, 14092.
- (16) Powers, D. C.; Ritter, T. *Nat. Chem.* **2009**, *1*, 302.
- (17) Cotton, F. A.; Koshevoy, I. O.; Lahuerta, P.; Murillo, C. A.; Sanau, M.; Ubeda, M. A.; Zhao, Q. *J. Am. Chem. Soc.* **2006**, *128*, 13674.
- (18) Cotton, F. A.; Gu, J. D.; Murillo, C. A.; Timmons, D. J. *J. Am. Chem. Soc.* **1998**, *120*, 13280.
- (19) Blake, A. J.; Gordon, L. M.; Holder, A. J.; Hyde, T. I.; Reid, G.; Schröder, M. *J. Chem. Soc., Chem. Commun.* **1988**, 1452.
- (20) Blake, A. J.; Holder, A. J.; Hyde, T. I.; Schröder, M. *J. Chem. Soc., Chem. Commun.* **1987**, 987.
- (21) Mirica, L. M.; Khusnutdinova, J. R. *Coord. Chem. Rev.* **2013**, 299.
- (22) Khusnutdinova, J. R.; Rath, N. P.; Mirica, L. M. *J. Am. Chem. Soc.* **2010**, *132*, 7303.
- (23) Tang, F.; Qu, F.; Khusnutdinova, J. R.; Rath, N. P.; Mirica, L. M. *Dalton Trans.* **2012**, *41*, 14046.
- (24) Khusnutdinova, J. R.; Rath, N. P.; Mirica, L. M. *J. Am. Chem. Soc.* **2012**, *134*, 2414.
- (25) Tang, F.; Zhang, Y.; Rath, N. P.; Mirica, L. M. *Organometallics* **2012**, *31*, 6690.
- (26) Khusnutdinova, J. R.; Rath, N. P.; Mirica, L. M. *Angew. Chem., Int. Ed.* **2011**, *50*, 5532.
- (27) Luo, J.; Khusnutdinova, J. R.; Rath, N. P.; Mirica, L. M. *Chem. Commun.* **2012**, *48*, 1532.
- (28) Connelly, N. G.; Geiger, W. E. *Chem. Rev.* **1996**, *96*, 877.
- (29) Foley, S. R.; Stockland, R. A., Jr.; Shen, H.; Jordan, R. F. *J. Am. Chem. Soc.* **2003**, *125*, 4350.
- (30) Rulke, R. E.; Ernsting, J. M.; Spek, A. L.; Elsevier, C. J.; van Leeuwen, P. W. N. M.; Vrieze, K. *Inorg. Chem.* **1993**, *32*, 5769.
- (31) Moriguchi, T.; Kitamura, S.; Sakata, K.; Tsuge, A. *Polyhedron* **2001**, *20*, 2315.
- (32) Constable, E. C.; King, A. C.; Raithby, P. R. *Polyhedron* **1998**, *17*, 4275.
- (33) SADABS; Bruker Analytical X-Ray, Madison, WI, 2008.
- (34) Sheldrick, G. M. *Acta Crystallogr.* **2008**, *A64*, 112.
- (35) See the Supporting Information.
- (36) de Graaf, W.; Boersma, J.; Smeets, W. J. J.; Spek, A. L.; van Koten, G. *Organometallics* **1989**, *8*, 2907.
- (37) Steffen, W. L.; Palenik, G. J. *Inorg. Chem.* **1976**, *15*, 2432.
- (38) Stephen, E.; Blake, A. J.; Carter, E.; Collison, D.; Davies, E. S.; Edge, R.; Lewis, W.; Murphy, D. M.; Wilson, C.; Gould, R. O.; Holder, A. J.; McMaster, J.; Schröder, M. *Inorg. Chem.* **2012**, *51*, 1450.
- (39) Bennett, M. A.; Canty, A. J.; Felixberger, J. K.; Rendina, L. M.; Sunderland, C.; Willis, A. C. *Inorg. Chem.* **1993**, *32*, 1951.
- (40) Canty, A. J.; Jin, H.; Skelton, B. W.; White, A. H. *Inorg. Chem.* **1998**, *37*, 3975.
- (41) Zhao, X. D.; Dong, V. M. *Angew. Chem., Int. Ed.* **2011**, *50*, 932.
- (42) Stephen, E.; Blake, A. J.; Carter, E.; Collison, D.; Davies, E. S.; Edge, R.; Lewis, W.; Murphy, D. M.; Wilson, C.; Gould, R. O.; Holder, A. J.; McMaster, J.; Schröder, M. *Inorg. Chem.* **2012**, *51*, 1450.
- (43) Lanci, M. P.; Remy, M. S.; Kaminsky, W.; Mayer, J. M.; Sanford, M. S. *J. Am. Chem. Soc.* **2009**, *131*, 15618.
- (44) Liu, G.-X.; Puddephatt, R. J. *Inorg. Chim. Acta* **1996**, *251*, 319.
- (45) Byers, P. K.; Canty, A. J.; Skelton, B. W.; White, A. H. *Organometallics* **1990**, *9*, 826.
- (46) Racowski, J. M.; Sanford, M. S. *Top. Organomet. Chem.* **2011**, *35*, 61.
- (47) Lin, T.-P.; Gabbai, F. P. *J. Am. Chem. Soc.* **2012**, *134*, 12230.
- (48) Cook, T. R.; McCarthy, B. D.; Lutterman, D. A.; Nocera, D. G. *Inorg. Chem.* **2012**, *51*, 5152.
- (49) Teets, T. S.; Cook, T. R.; McCarthy, B. D.; Nocera, D. G. *Inorg. Chem.* **2011**, *50*, 5223.